RSC Advances

PAPER

View Article Online
View Journal | View Issue

Cite this: *RSC Adv.*, 2020, **10**, 17461

Synthesis and gas permeation properties of thermally rearranged poly(ether-benzoxazole)s with low rearrangement temperatures

Yunhua Lu, *[a] Jianhua Zhang,[a] Guoyong Xiao,[a] Lin Li,[b] Mengjie Hou,[b] Junyi Hu[a] and Tonghua Wang*[b]

The diamine monomer, 9,9-bis[4-(4-amino-3-hydroxylphenoxy)phenyl] fluorene (bis-AHPPF) was successfully synthesized according to our modified method. A series of hydroxyl-containing poly(ether-imide)s (HPEIs) were prepared by polycondensation of the bis-AHPPF diamine with six kinds of dianhydrides, including 1,2,3,4-cyclobutanetetracarboxylic dianhydride (CBDA), pyromellitic dianhydride (PMDA), 3,3′,4,4′-biphenyl tetracarboxylic diandhydride (BPDA), 3,3′,4,4′-oxydiphthalic anhydride (ODPA), 3,3′,4,4′-benzophenonetetracarboxylic dianhydride (BTDA) and 4,4′-(hexafluoroisopropylidine)diphtalic anhydride (6FDA) followed by thermal imidization. The corresponding thermally rearranged (TR) membranes were obtained by solid state thermal treatment at high temperature under a nitrogen atmosphere. The chemical structure, and physical, thermal and mechanical properties of the HPEI precursors were characterized. The effects of heat treatment temperature and dianhydrides on the gas transport properties of the poly(ether-benzoxazole) (PEBO) membranes were also investigated. It was found that these HPEIs showed excellent thermal and mechanical properties. All the HPEI precursors underwent thermal conversion in a N_2 atmosphere with low rearrangement temperatures. The gas permeabilities of the PEBO membranes increased with the increase of thermal treatment temperature. When HPEI–6FDA was treated at 450 °C for 1 h, the H_2, CO_2, O_2 and N_2 permeabilities of the membrane reached 239.6, 196.04, 46.41 and 9.25 Barrers coupled with a O_2/N_2 selectivity of 5.02 and a CO_2/N_2 selectivity of 21.19. In six TR-PEBOs, PEBO–6FDA exhibited the lowest rearrangement temperature and largest gas permeabilities. Therefore, thermally rearranged membranes from bis-AHPPF-based HPEIs are expected to be promising materials for gas separation.

Received 7th January 2020
Accepted 25th April 2020

DOI: 10.1039/d0ra00145g

rsc.li/rsc-advances

1. Introduction

Membrane technology has played a key role in many fields including gas separation, water treatment, fuel cells, *etc.*[1–3] The use of polymeric membranes in gas separation applications have been investigated in order to solve problems such as nitrogen and oxygen enrichment from air, purity of natural gas, SO_2 removal from flue gas, separation of organic gas mixtures and CO_2 capture for solving global warming.[4–6] In commercial polymers, polyimides (PIs) are employed for some special applications due to their excellent thermal resistance, chemical resistance and mechanical properties.[7–10] The structure design and synthesis of polyimides are very flexible, so there are many kinds of polyimides to meet the different application requirements. Among polyimides, hydroxyl-containing polyimides (HPIs), as reactive polymers, can be further functionalized to prepare photosensitive polyimides, organic–inorganic polyimide composites, and thermo-crosslinkable polyimides, which are expected to be applied in optical films, electronic packaging, liquid crystal displays, photoelectric functional devices, gas separation membranes and other fields.[11–14]

In recent years, HPI, as the precursor of thermally rearranged (TR) polymers, has been widely concerned and investigated.[15] After thermal rearrangement reaction in solid state at 350–450 °C, the benzoxazole structure from HPI was formed, accompanied by the emission of CO_2. The obtained TR polymers are a kind of microporous polymer with high fractional free volume (FFV) and narrow cavity size distribution, resulting in high gas permeabilities and outstanding separation selectivities even beyond the 2008 Robeson limit.[16–20] Hence, there is a strong incentive for development of new TR polymers with high gas permeability and selectivity. Currently, in order to synthesize TR polymers, two main steps are usually involved: (i) synthesis of HPI precursors using thermal, azeotropic or chemical imidization methods, and (ii) thermal conversion of the HPI precursors into polybenzoxazoles (PBOs) in solid

[a]School of Chemical Engineering, University of Science and Technology Liaoning, Anshan, Liaoning, 114051, P. R. China. E-mail: lee.lyh@163.com; Fax: +86 412 5216702; Tel: +86 412 5929952

[b]School of Chemical Engineering, Dalian University of Technology, Dalian, Liaoning 116024, P. R. China. E-mail: wangth@dlut.edu.cn

state.[21–24] Although the imidization methods usually lead to the final TR polymers with the same chemical structure, the physical and gas separation properties of the TR polymers were very different.[25–29] Therefore, the structure and properties of TR polymers could be easily adjusted by molecular structure design and preparation methods to facilitate specific gas separation applications.[30–35] According to the reported literatures,[25–35] HPI is the most commonly used precursor for the preparation of TR polymers, and most of TR polymers are based on HPI precursors made from 4,4′-(hexafluoroisopropylidene)diphthalic anhydride (6FDA) and 2,2′-bis(3-amino-4-hydroxyphenyl)-hexafluoropropane (APAF) or 3,3′-dihydroxy-4,4′-diaminobiphenyl (HAB). Later, spiro, cardo and triptycene based TR polymers have also been reported in succession.[35]

Generally speaking, the monomers with rigid backbone, bulky bridging and pendant groups should be preferred to endow TR polymers with high FFV and gas permeabilities. However, the HPIs with rigid structures usually need a relatively higher thermal rearranged temperature (T_{TR}), which is not cost-effective and poor mechanical properties in application. Furthermore, the low-T_{TR} TR polymers containing very flexible backbone generally bring a higher rate of conversion and lower gas permeabilities.[36] Therefore, the structure design and synthesis of TR polymers need to consider the balance between chain rigidity and flexibility, and the trade-off relationship between the production cost and the separation performance.

As reported, 9,9-bis(3-amino-4-hydroxyphenyl)fluorene (bisAHPF) is a kind of diamine with rigid and bulky fluorenyl cardo group, which has been used as the hydroxy-functional diamine to prepare the TR polymers.[37–39] Cardo moiety with loop shaped structure in polymer main chains is useful to improve the FFV and gas permeabilities of polymeric membranes.[40–44] Additionally, fluorenyl cardo group has a large steric hindrance, which is beneficial to restrict the tight stacking of macromolecular chains and increase chain rigidity, thermal properties and FFV. Unfortunately, HPIs from bisAHPF need a higher T_{TR} temperature, resulting in poor mechanical properties as well as processability, so copolymerization with other diamine has been adopted to improve the properties of final TR materials.[37–39]

In the present study, we report the synthesis and gas transport properties of a series of poly(ether-benzoxazole) (PEBO) membrane prepared from hydroxyl-containing poly(ether-imide)s (HPEIs). The HPEIs were prepared by a polycondensation reaction between 9,9-bis[4-(4-amino-3-hydroxylphenoxy)phenyl]fluorene (bis-AHPPF) and six kinds of dianhydrides, followed by thermal imidization. After subsequently thermally treated in N_2 atmosphere, the corresponding PEBOs were obtained for gas separation. Here, 9,9-bis[4-(4-amino-3-hydroxylphenoxy)phenyl]fluorene contains both flexible ether linkage and bulky cardo moiety, which is expected to endow HPEI moderate rigidity to decrease the T_{TR} and maintain a higher gas permeabilities. Finally, the alteration of structure, physical properties as well as gas separation properties of HPEI and PEBO membranes were systematically characterized by numbers of proper analytic techniques. It is believed that this work would provide some valuable insights to design and prepare the gas separation membrane materials for energy development and environmental protection.

2. Experimental

2.1. Materials

9,9-Bis(4-hydroxylphenyl)fluorene (Bis-HPF) was provided by Huanghua Xinnuo Lixing Fine Chemical Stock Co. Ltd. (China). 5-Fluoro-2-nitrophenol was bought from Shanghai bide pharmatech Ltd. (China). 1,2,3,4-Cyclobutane tetracarboxylic dianhydride (CBDA) was obtained from Liaoning Oxiran Huahui New Materials Co., Ltd. (China). 4,4′-(Hexafluoroisopropylidene)diphthalic anhydride (6FDA), 3,3′,4,4′-biphenyltetracarboxylic dianhydride (BPDA), 4,4′-oxydiphthalic anhydride (ODPA) and 3,3′,4,4′-benzophenonetetracarboxylic dianhydride (BTDA) were purchased from Chinatech (Tianjin) Chemical Co., Ltd. (China). Pyromellitic dianhydride (PMDA), Pd/C (10% Pd), hydrazine hydrate, anhydrous potassium carbonate (K_2CO_3), *N*,*N*-dimethylformamide (DMF) and *N*,*N*-dimethylacetamide (DMAc) were obtained from Sinopharm Chemical Reagent Co. Ltd. (China). All dianhydrides were dried in a vacuum oven at 180 °C for 12 h before use. All solvents were of reagent-grade quality and used without further purification.

2.2. Monomer synthesis

The ether-containing bis(*o*-aminophenol) monomer, 9,9-bis[4-(4-amino-3-hydroxyl phenoxy)phenyl]fluorene (bis-AHPPF) was synthesized in two steps, according to our previously reported method, from 9,9-bis(4-hydroxylphenyl)fluorene and 5-fluoro-2-nitrophenol by nucleophilic aromatic substitution in the presence of potassium carbonate (K_2CO_3) and DMF as solvent, followed by catalytic reduction with hydrazine hydrate and Pd/C as catalyst.[45] ^{1}H NMR and FTIR spectroscopic techniques were used to prove the chemical structures of the intermediate dinitro compounds and the final hydroxyl-containing diamine. 9,9-Bis[4-(4-nitro-3-hydroxylphenoxy)phenyl]fluorene (bis-NHPPF). FTIR (KBr, cm^{-1}): 3060 (O–H), 1627, 1529 (C=C), 1578, 1322 (–NO_2), 822, 724 (C–H). ^{1}H NMR (500 MHz, DMSO-d_6) δ: 11.14 (s, 2H), 7.97 (td, J = 6.1, 3.0 Hz, 4H), 7.52 (d, J = 7.7 Hz, 2H), 7.45 (t, J = 7.4 Hz, 2H), 7.38 (t, J = 7.5 Hz, 2H), 7.26–7.20 (m, 4H), 7.13–7.08 (m, 4H), 6.52 (dd, J = 9.1, 7.2 Hz, 4H). 9,9-Bis[4-(4-amino-3-hydroxylphenoxy)phenyl]fluorene (bis-AHPPF). FTIR (KBr, cm^{-1}): 3380, 3306 (N–H), 3062 (O–H), 1606, 1509 (C=C), 1342, 1281(C–N), 822, 740 (C–H). ^{1}H NMR (500 MHz, DMSO-d_6) δ: 9.26 (s, 2H), 7.91 (d, J = 7.5 Hz, 2H), 7.45–7.36 (m, 4H), 7.31 (t, J = 7.5 Hz, 2H), 7.03 (d, J = 8.8 Hz, 4H), 6.75 (d, J = 8.9 Hz, 4H), 6.55 (d, J = 8.3 Hz, 2H), 6.34 (d, J = 2.6 Hz, 2H), 6.26 (dd, J = 8.4, 2.6 Hz, 2H), 4.38 (s, 4H).

2.3. Synthesis of hydroxyl-containing poly(ether-imide)s

The hydroxyl-containing poly(ether-imide) (HPEI) precursors based on bis-AHPPF and six kinds of dianhydrides including CBDA, PMDA, BPDA, ODPA, BTDA and 6FDA were prepared *via* a two-step thermal imidization process, as shown in Scheme 1. Taking the synthesis of HPEI–6FDA as an example: bis-AHPPF (0.01 mol, 5.6463 g) and DMAc (61 mL) were added into

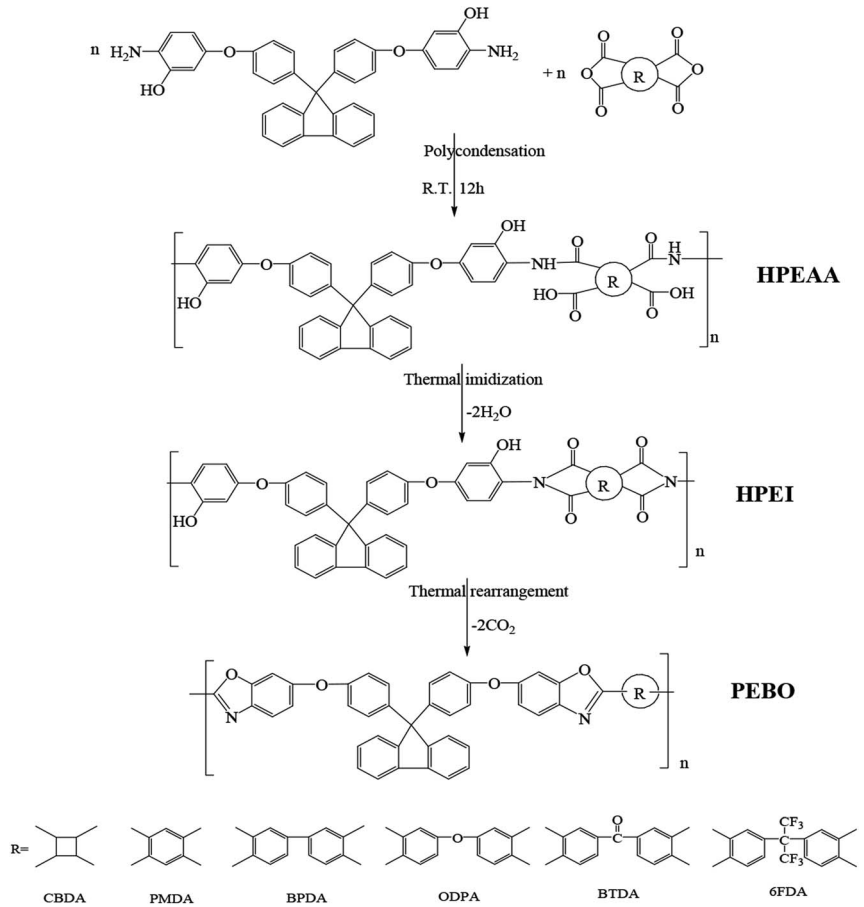

Scheme 1 Preparation of PEBO *via* thermal rearrangement.

a two-neck 250 mL flask equipped with a mechanical stirrer at 0–10 °C. After the diamine monomer was dissolved completely, 6FDA (0.01 mol, 4.4424 g) was added. The reaction mixture was stirred continuously at room temperature for 12 h to form a viscous hydroxyl containing poly(ether-amic acid) (HPEAA) solution with a concentration of 15 wt%. Then, the HPEAA solution was directly casted onto clean glass plates, followed by drying at 40 °C for 3 hours to evaporate the most solvent slowly. After that, it was further dried at 80 °C for 1 h, 150 °C for 1 h, 200 °C for 1 h and 250 °C for 15 min in a far-infrared oven. Finally, the HPEI–6FDA membrane was peeled off glass plates by immersion in hot deionized water and dried in a vacuum at 100 °C for 24 h. According to the same procedure, HPEI–CBDA, HPEI–PMDA, HPEI–BPDA, HPEI–ODPA and HPEI–BTDA were also prepared.

2.4. Preparation of TR-PEBO membranes

The TR-PEBO membranes were prepared by thermal rearrangement of the HPEI precursor under a high-purity nitrogen atmosphere (200 mL min^{-1}), as shown in Scheme 1. HPEI-6FDA were sandwiched between two graphite plates to avoid deformation during thermal treatment, and placed into a tube furnace. Then, the furnace was heated up to 350, 400 and 450 °C at a heating rate of 3 °C min^{-1} and held for 1 hour to perform the thermal rearrangement separately. Finally, the furnace was cooled down to room temperature naturally. The obtained TR polymers were called as HPEI–6FDA-350, HPEI–6FDA-400 and HPEI–6FDA-450. Similarly, other HPEIs were also thermally treated at 450 °C for 1 hour to obtain TR-PEBO membranes, which were named as PEBO–CBDA, PEBO–PMDA, PEBO–BPDA, PEBO–ODPA, PEBO–BTDA and PEBO–6FDA, respectively.

2.5. Measurements

Fourier transform infrared (FTIR) measurements were performed with an instrument Nicolet iS 10 spectrometer from 500 to 4000 cm^{-1}. The ^{1}H-NMR analyses of dinitro compound and diamine monomer were conducted on an Agilent-500 spectrometer (Agilent Technologies, USA) at 500 MHz, and deuterated dimethyl sulfoxide (DMSO) was used as solvent and tetramethylsilane as internal reference. X-ray photoelectron spectroscopy (XPS) spectra of PEBO-6FDA were determined by an ESCALAB 250Xi spectrometer (Thermo Fisher, USA).

Dynamic mechanical properties of HPEIs were tested by DMA 8000 (Perkin Elmer, USA) from 50 to 400 °C at a rate of 10 °C min^{-1} with 1HZ in air and N_2 atmosphere (80 mL min^{-1}). Glass transition temperatures (T_g) of PEBOs were carried out using a Perkin Elmer Instruments DSC 4000 with a heating rate of 20 °C min^{-1} in nitrogen atmosphere. Two

heating–cooling cycles from 50 °C to 400 °C were performed, and T_g was determined based on the second heating cycle. Thermogravimetric-mass spectrometry (TG-MS) was conducted on the Netzsch STA 449F3 (Germany) with a heating rate of 10 °C min^{-1} and a nitrogen purge of 50 mL min^{-1} to evaluate thermal stability characteristics as well as the thermal rearrangement, in the temperature range from room temperature to 900 °C.

The densities of HPEIs were measured by the Shimadzu MH-124S Densitometer (Japan). Density for each HPEI sample was measured for at least three times and the average value was used for the FFV calculation. FFV of each polymer was calculated based on the following eqn (1):

$$\mathrm{FFV} = \frac{V_o - 1.3V_w}{V_o} \quad (1)$$

where V_o is the molar volume of the polymer (volume per unit mass or mole of repeat unit) which is obtained from experimental measurement of polymer density at a certain temperature (typically 30 °C), and V_w is the van der Waals volume, which is calculated according to the Bondi's group contribution method.[46]

Wide-angle X-ray diffraction (WAXD) patterns were recorded at room temperature (about 25 °C) by X'Pert Powder X-ray diffractometer (PANalytical, Almelo, Netherlands) to show the changes in intersegmental properties of these polymers. The 2θ value changed from 5° to 70° with copper K_α radiation (operating at 40 kV and 40 mA). The average d-spacing values of the HPEI and PEBO were calculated by means of Bragg's law using eqn (2):

$$n\lambda = 2d \sin\theta \quad (2)$$

where n is an integral which is equal to 1, λ is the wavelength of the Cu source (1.54 Å), θ represents the diffraction angle and d represents the average spacing between polymer chain.

Mechanical properties (tensile strength, Young modulus, and elongation at break) of HPEI precursors were measured by using the HY-0580 stretching tester (Shanghai Hengyi Precision Instrument Co., Ltd., China) fitted with a 100 N load at room temperature. The samples of 1 cm width and 7 cm length were clamped at both ends with an initial gauge length of 5 cm, and the elongation rate was of 10 mm min^{-1}.

Single gas permeation of PEBO membranes was tested by traditional variable volume-constant pressure method using high purity gases (>99.99%), *i.e.*, H_2 (2.89 Å), CO_2 (3.3 Å), O_2 (3.46 Å) and N_2 (3.64 Å). The GC analysis was conducted by GC7890 (Techcomp Ltd.) equipped with a thermal conductivity detector (TCD) and a packed column. For each membrane, the measurements were under taken for more than three samples prepared under the same conditions. The reported permeation data are the averaged value with a measurement precision of 10%. For the details of the test procedure, please refer to our previous report.[45] In the study, the feed pressure and testing temperature were maintained at 0.01 or 0.1 MPa and 30 °C, respectively. The gas permeabilities were determined from the eqn (3).

$$P = \frac{FL}{S\Delta P} \quad (3)$$

where P is the permeability in Barrer (1 Barrer $= 1 \times 10^{-10}$ cm^3 (STP) cm cm^{-2} s^{-1} cmHg), F, ΔP, S and L are the flux of permeable gas, the partial pressure difference of the gas across the tested membrane, the effective permeation area and the thickness of the tested membrane, respectively. The ideal selectivity of a membrane for gas A to gas B is given in eqn (4).

$$\alpha_{A/B} = P_A/P_B \quad (4)$$

3. Results and discussion

3.1. Monomer synthesis

The flexible ether-containing bis(*o*-aminophenol) monomer, 9,9-bis[4-(4-amino-3-hydroxylphenoxy)phenyl]fluorene was synthesized in two steps, by K_2CO_3 mediated nucleophilic substitution reaction of 9,9-bis(4-hydroxylphenyl)fluorene and 5-fluoro-2-nitrophenol, followed by catalytic reduction with hydrazine hydrate and Pd/C as catalyst. FTIR and ^{1}H NMR results identified the chemical structures of the intermediate dinitro compound and the final hydroxyl diamine monomer, which were reported in our previous literature.[45]

3.2. Synthesis and characterization of HPEI precursors

The images of the HPEIs and PEBO-6FDA were photographed, as shown in Fig. 1. All HPEIs were yellow or brown. After thermal treatment at 450 °C, the color of membrane turned black, but the PEBO-6FDA was still flexible to meet the following characterization.

The HPEIs were synthesized from the cardo diamine bis-AHPPF and six kinds of dianhydrides including CBDA, PMDA, BPDA, ODPA, BTDA and 6FDA *via* a two-step thermal imidization method. After that, most DMAc solvent was removed and the ring-closure reaction was partly completed. The HPEIs are readily prepared with flexible and good mechanical strengths for the further tests. The FTIR spectra for HPEIs, shown in Fig. 2, confirmed the imidization. All HPEIs exhibited the characteristic imide group absorptions at around 1779 and 1717 cm^{-1} for imide carbonyl symmetrical and asymmetrical stretching, approximately 1388 cm^{-1} for C–N stretching of imide ring, and around 743 cm^{-1} for C–N–C ring deformation. In addition, the characteristic broad peak of O–H group appeared at 3000–3600 cm^{-1}. The band around at 1213 cm^{-1} was the asymmetrical stretching vibration of C–O bonds. The spectra have evidenced the existence of typical imide groups and other functional groups in the molecular structure of HPEI precursors.

Glass transition temperatures (T_g) of HPEIs are determined by DMA 8000 in air or N_2, and Fig. 3(a) and (b) displays the tanδ–T curves of HPEIs. The temperature at which the maximum of loss tangent (tanδ) observed is commonly defined as the T_g value by DMA test, as shown in Table 1. As expected, with increasing rigidity of dianhydride monomer, the T_g values are shifted toward higher temperature region. The ether connecting

Fig. 1 Images of HPEIs and PEBO–6FDA membranes.

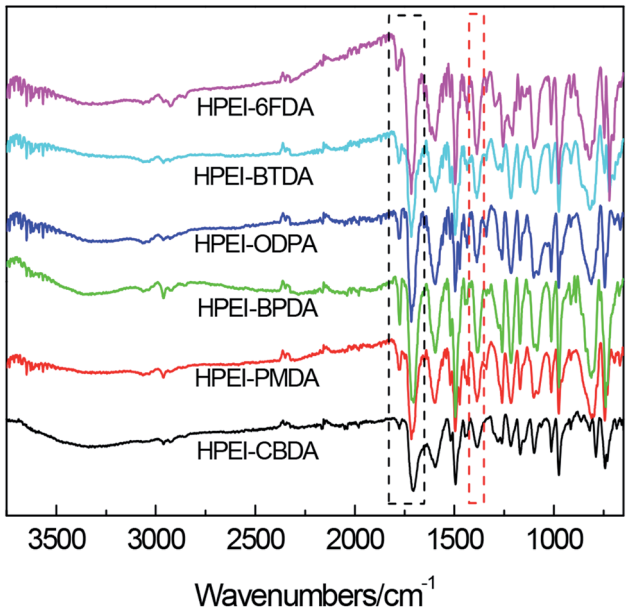

Fig. 2 FTIR spectra of HPEIs.

group can increase the mobility of the macromolecular chains, while bulky fluorene moiety hinders the chain motion. Moreover, hydrogen bonding might further increase the interaction between molecular chains to limit the chain movement. As a result, the T_g values of HPEIs are almost above 300 °C. Furthermore, the HPEI–6FDA shows a higher T_g value compared with the reported HPEI (280 °C, DSC) from 6FDA and 2,2-bis(4-(4-amino-3-hydroxyphenoxy)phenyl)hexafluoropropane (6FBAHPP).[36] It may be attributed to the stronger rigidity and larger volume of fluorene group than that of hexafluoroisopropyl group.

Using DMA to study the HPEIs not only provides an alternative and accurate method for T_g (α relaxation, glass–rubber transition) measurement, but also offers some other information on thermal behavior. The β and γ relaxations corresponding to the subglass relaxation of the local mobility have been observed in Fig. 3(a) and (b). For HPEIs, because of the further thermal imidization reaction at 200–300 °C, and thermal rearrangement as well as crosslinking above 350 °C, the tanδ–T curves were complex. In Fig. 3(a), because of some small molecules produced by the thermal decomposition reaction, the tanδ peak moves slightly to the low temperature direction. However, the tanδ peak of HPEI–BTDA shifted to high temperature, indicating that the thermal crosslinking reaction took place. After the α relaxation peak of HPEI–ODPA, another lower tanδ loss peak appeared, which might mean that the thermal crosslinking in air reduced the mobility of molecular segments and increased the rigidity of the molecular chain. Due to the testing temperature of 50–400 °C, this phenomenon of other HPEIs is not fully displayed, only some trends can be seen. As shown in Fig. 3(b), thermal oxidation reaction is avoided as much as possible, so the tanδ–T curves measured under nitrogen condition are different from those measured in air. For HPEI–BPDA, HPEI–ODPA and HPEI–6FDA, the T_g values in N_2 were higher than those obtained in air because of more complete imidization without oxidative decomposition. The T_g of HPEI–BTDA decreased from 370 °C to 335 °C due to no

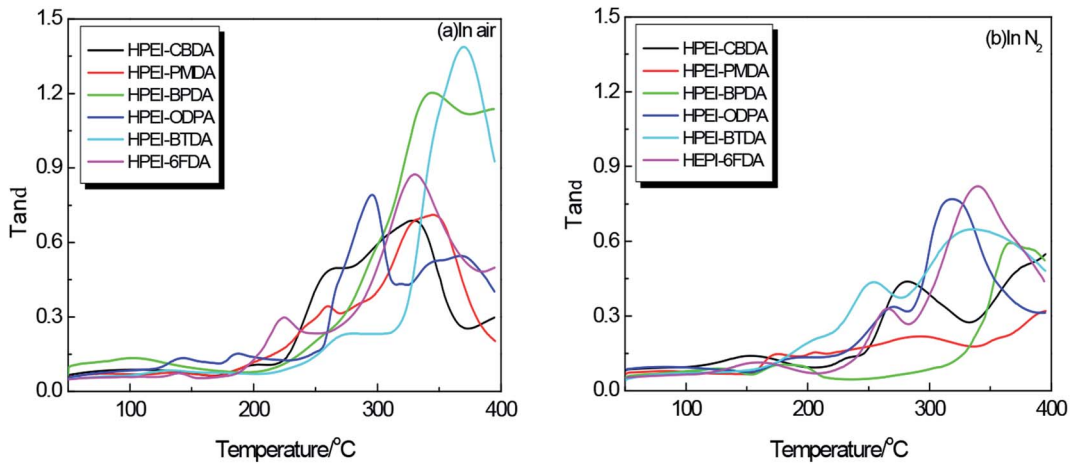

Fig. 3 Tanδ–T curves of HPEIs (a) in air; (b) in N_2.

Table 1 Thermal and mechanical properties of HPEI samples

Samples	T_g[a] (°C) DMA N_2	T_g[a] (°C) DMA Air	T_{d5}[b] (°C)	T_{d10}[b] (°C)	T_{TR}[c] (°C)	R_{700}[d] (%)	Tensile strength (MPa)	Young modulus (GPa)	Elongation at break (%)
HPEI–CBDA	—[e]	330	274	356	372	59	126.9 ± 2.0	4.4 ± 0.2	3.6 ± 0.2
HPEI–PMDA	—[e]	345	337	377	387	61	99.3 ± 4.0	3.8 ± 0.1	3.2 ± 0.1
HPEI–BPDA	366	343	307	387	403	65	111.2 ± 3.0	4.1 ± 0.2	3.6 ± 0.1
HPEI–ODPA	318	295	296	365	378	60	103.2 ± 3.0	3.7 ± 0.1	3.3 ± 0.3
HPEI–BTDA	335	370	311	379	393	63	86.5 ± 4.0	4.5 ± 0.2	2.0 ± 0.1
HPEI–6FDA	339	330	326	373	371	62	126.8 ± 3.0	3.7 ± 0.1	4.3 ± 0.2

[a] T_g: glass transition temperature measured by DMA. [b] T_{d5} and T_{d10}: 5% and 10% weight loss temperatures in TGA at 10 °C min^{-1} heating rate under a nitrogen atmosphere, respectively. [c] T_{TR}: thermal rearrangement temperature obtained from DTG–T curves at the maximum conversion rate. [d] R_{700}: residual yield in TGA at 700 °C under a nitrogen atmosphere. [e] Not estimated in tanδ–T curves in N_2.

thermal oxidative crosslinking. Nevertheless, the largest tanδ loss peaks of HPEI–CBDA and HPEI–PMDA didn't appear until 400 °C, so their T_gs were not estimated.

The stress–strain curves of HPEI samples are illustrated in Fig. 4, and the corresponding data are given in Table 1. These HPEI samples showed excellent tensile strength and Young modulus. According to the shape of stress–strain curves, the HPEIs still exhibited the character of brittle materials with lower elongation at break and no yield point. The elongation of these HPEIs was relatively lower than some commercial PI films such as Kapton, although there were flexible ether bonds in the main chain of polymer. The reason may be that the steric resistance of fluorene group increased the rigidity of macromolecular chain and the membrane was not biaxially stretched. Among them, HPEI–CBDA and HPEI–6FDA showed higher tensile strength about 127 MPa, while HPEI–6FDA exhibited the biggest elongation with 4.3%. Excellent mechanical properties can ensure that they can withstand subsequent heat treatment and testing.

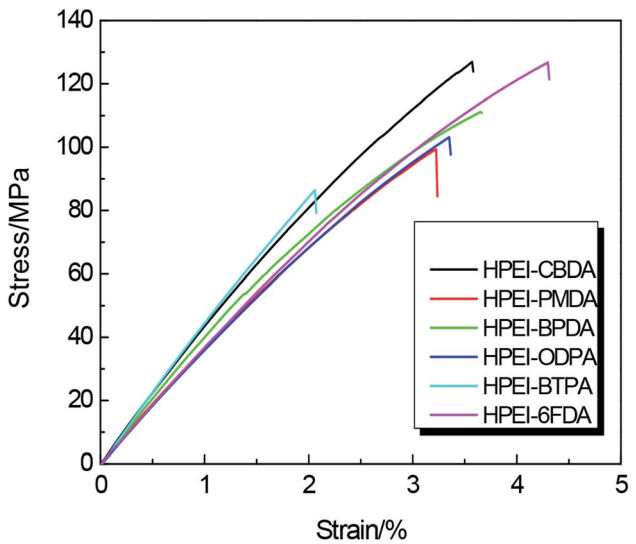

Fig. 4 Stress–strain curves of HPEI samples.

As we known, enhancing the fractional free volume (FFV) of polymer was proved to be beneficial to improving the gas permeability of membrane.[4] Table 2 summarizes the densities and fractional free volumes (FFVs) of HPEIs. Although the thermal cyclization process was incomplete, we assumed that the imidization degree was 100% to compare the effect of repeat unit structure on FFV. The density data of the samples were measured, and the FFV was calculated from eqn (1). These HPEIs were expected to exhibit higher FFVs because the incorporation of the rigid and bulky cardo moiety into the polymer chain induced loose chain packing and led to an increase in the d-spacing. However, the introduction of ether linkages increased the flexibility of macromolecular chains and reduced the distance between molecular chains as well as FFV. As a result, the FFVs of these HPEIs were not very high. Comparatively, HPEI–6FDA showed the highest FFV due to the hexafluoroisopropyl group with steric hindrance effect.

3.3. Thermal rearrangement of HPEI into poly(ether-benzoxazole)(PEBO)

As shown in Fig. 5, FTIR spectra are provided for the PEBOs, and the spectra of HPEI–ODPA is used to compare and indicate the change of chemical structure. It can be seen from all spectra that the characteristic C=O of the imide group at 1785 and 1725 cm^{-1} almost disappeared or obviously decreased. Instead, –N=C–O stretching bands in benzoxazole were observed at 1050 and 1557 cm^{-1} after thermal treatment at 450 °C for 1 h, which indicated that the rearrangement reaction had taken place.

The thermal behavior and rearrangement mechanism of HPEI precursors were studied by TGA-MS in N_2 atmosphere, and the T_d and T_{TR} observed from Fig. 6 was given in Table 1. As previously reported, the thermal rearrangement of hydroxyl-imide to benzoxazoles ring accompanied the evolution of carbon dioxide (2 mol CO_2/HPEI repeating unit). All HPEIs in this study exhibited three weight losses, the first small mass loss around 280 °C was induced by thermal imidization; the second larger weight loss at the range of 325 to 450 °C, was caused by thermal conversion from HPEI to PEBO, where the amount of CO_2 evolution reached the maximum value at about

Table 2 Physical properties of HPEI precursors

Polymers[a]	Density (g cm^{-3})	Molar mass, M_0[b] (g mol^{-1})	Molar volume, V_0 (cm^3 mol^{-1})	Van der Waals volume, V_w (cm^3 mol^{-1})	Fractional free volume, FFV[c]	d-Spacing (nm)
HPEI–CBDA	1.2423	724	583.3	407.9	0.091	0.47
HPEI–PMDA	1.3789	746	541.0	379.2	0.089	0.43
HPEI–BPDA	1.3636	822	602.8	423.5	0.087	0.42
HPEI–ODPA	1.3810	838	606.8	429.0	0.081	0.43
HPEI–BTDA	1.3697	850	620.6	435.2	0.088	0.44
HPEI–6FDA	1.2721	972	764.1	512.0	0.129	0.55

[a] Thermally cyclized at 250 °C for 15 min. [b] Estimated by assuming 100% imidization conversion. [c] Fractional free volume of polymer membranes by Bondi method as in eqn (1).

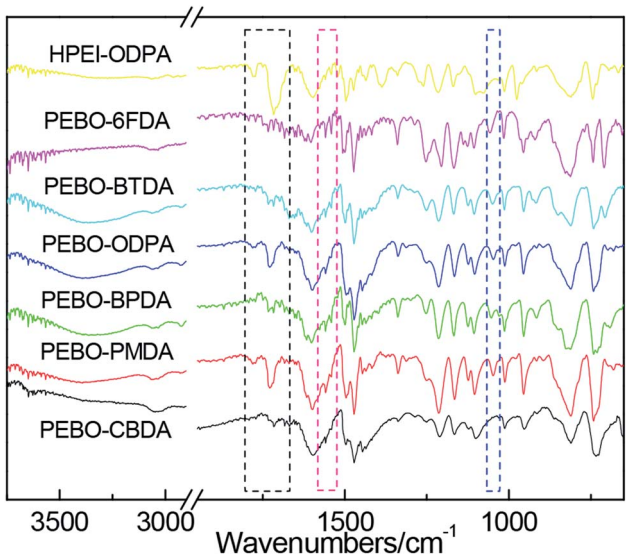

Fig. 5 FT-IR spectra of PEBO membranes.

400 °C as confirmed by MS.[15] In this paper, the thermal rearranged temperature (T_{TR}) of HPEIs was defined as the temperature at the maximum conversion rate for this polymer, which was closely related to the rigidity of the molecular chain. The T_{TR} of HPEI–6FDA was about 371 °C, lower than that of most precursors, such as 452 °C of HPI(HAB–6FDA), 430 °C of HPI(APAF–6FDA) and 411 °C of HPI(6FBAHPP–6FDA)[47] due to the synergistic effect of flexible linkage of –O– and large steric hindrance of fluorene moiety. The third distinct mass loss began at approximately 550 °C, which was caused by decomposition of the polymer backbone. Relatively, HPEI–CBDA showed the lowest thermal stability due to its semialiphatic ring structure although its T_{TR} was 372 °C. In general, all precursors exhibited a high residual weight of 59–65% at 700 °C. These experimental results indicate that the HPEIs with fluorene cardo moieties have been converted to PEBO successfully.

The intersegmental distances of membranes were characterized by wide-angle X-ray diffraction (WAXD). The corresponding XRD patterns of HPEIs and PEBOs are shown in Fig. 7(a) and (b), and the d-spacing values of HPEIs are also listed in Table 2. Actually, the FFV is closely related to the chain packing. The d-spacing results are in agreement with the FFV data in some degree, indicating that the fluorenyl moiety could provide a larger FFV for the polymer precursors. Both HPEIs and PEBOs exhibited broad amorphous peaks, which indicated the amorphous nature of these polymers. From Fig. 7(a), the d-spacing value of HPEI–6FDA is higher than that of other HPEI precursors, which is attributed to the large steric hindrance of hexafluoroisopropyl group to limit the tight packing of molecular chains. In contrast, the d-spacings of PEBO–PMDA, PEBO–BPDA, PEBO–ODPA and PEBO–BTDA increased slightly after the thermal rearrangement process(in Fig. 7(b)). The d-spacing value of PEBO–6FDA increased from 0.55 nm to 0.61 nm, while the d-spacing value of PEBO–CBDA decreased from 0.47 nm to 0.44 nm because of the poor thermal stability of alicyclic structure resulting in the breaking of the macromolecular backbone and the tight intermolecular chains packing. Therefore, these d-spacings may provide an indicator of the amount of available space to penetrate small molecules.

The XPS analysis of PEBO–6FDA is given to illustrate to change of chemical structure, as shown in Fig. 8, which shows the presence of C, N, O and F in the polymer. The fitting curves of C, O and N suggest that the benzoxazole ring structures have been formed from HPEI. Fig. 8(b) shows that there is N=C of benzoxazole ring at 287.2 eV. Moreover, according to literatures, 400.6 eV and 399.2 eV have been assigned to –N< in imide ring and –N= in benzoxazole ring.[37] According to Fig. 8(d), the two peaks at 400.4 eV and 399.1 eV indicate the PEBO–6FDA contain the imide group (–N<) and benzoxazole ring structure (–N=). Based on the areas of XPS fitting peaks, the degree of conversion can be calculated about 45.2%, which illustrates that HPEI has been partially converted to PEBO. Hence, thermal treatment time and temperature need to be further adjusted in order to obtain high TR conversion rate and gas permeability.[36,48]

The thermal properties of PEBOs are characterized and shown in Fig. 9. The T_g values were improved in varying degree and mainly around at 350 °C, while the effect of dianhydride structure on the T_g was very small. After high temperature treatment, thermal rearrangement of intramolecular and crosslinking of intermolecular could be induced, leading to the rigid molecular chain and strong interchain interaction accompanied with low segmental movement ability. The data

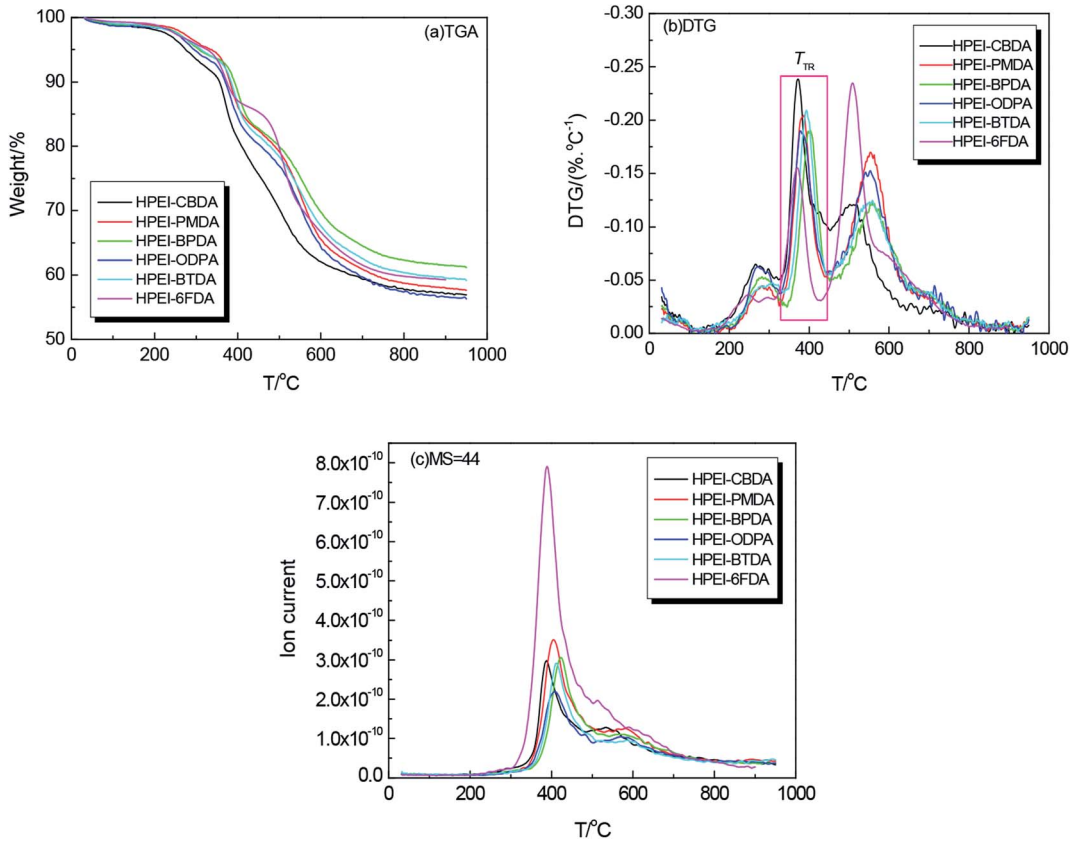

Fig. 6 TGA–DTG curves of HPEIs measured in N_2 (a)TGA curves; (b)DTG curves; (c) MS = 44 curves.

indicated that these PEBOs exhibited good thermal properties and could be used in high temperature environment.

3.4. Gas permeability and selectivity

In order to evaluate the gas transport properties, as well as the effects of thermal treatment temperature and dianhydrides on the separation performance of membranes, four single pure gas permeabilities of H_2, N_2, O_2, and CO_2 were tested by the constant-volume/variable-pressure method and the gas permeabilities (P) as well as the ideal separation factors of these PEBOs are listed in Tables 3 and 4. Based on the results of FFV and d-spacing, HPEI–6FDA was expected to exhibit the highest gas permeabilities, so it was selected as the research target for thermal treatment temperature. For HPEI–6FDA, the CO_2 permeability is 7.12 Barrer, while the O_2 permeability is 1.47 Barrer and N_2 permeability is 0.36 Barrer, with a CO_2/N_2 selectivity of 19.78 and an O_2/N_2 ideal selectivity of 4.08. Hence, HPEI–6FDA has a reasonable ideal selectivity, but the low gas permeability makes it unattractive as a gas separation membrane.

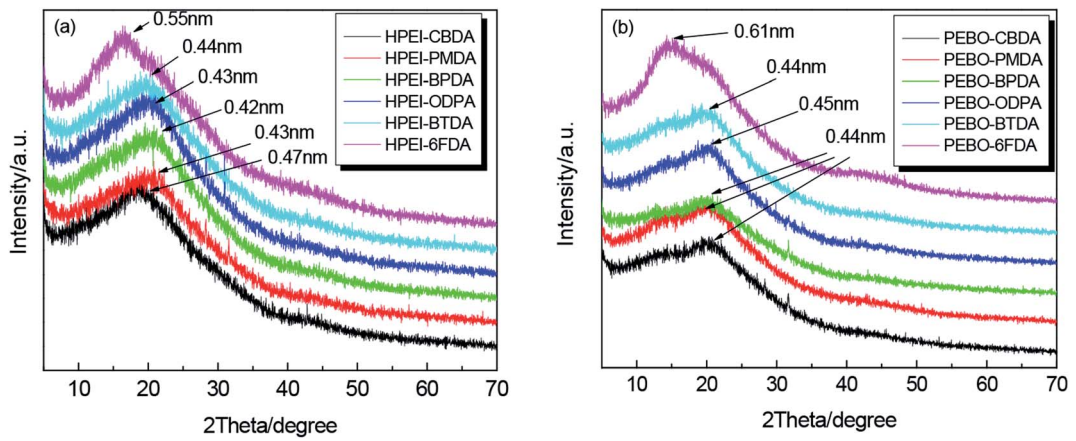

Fig. 7 XRD curves (a) HPEIs; (b) PEBOs.

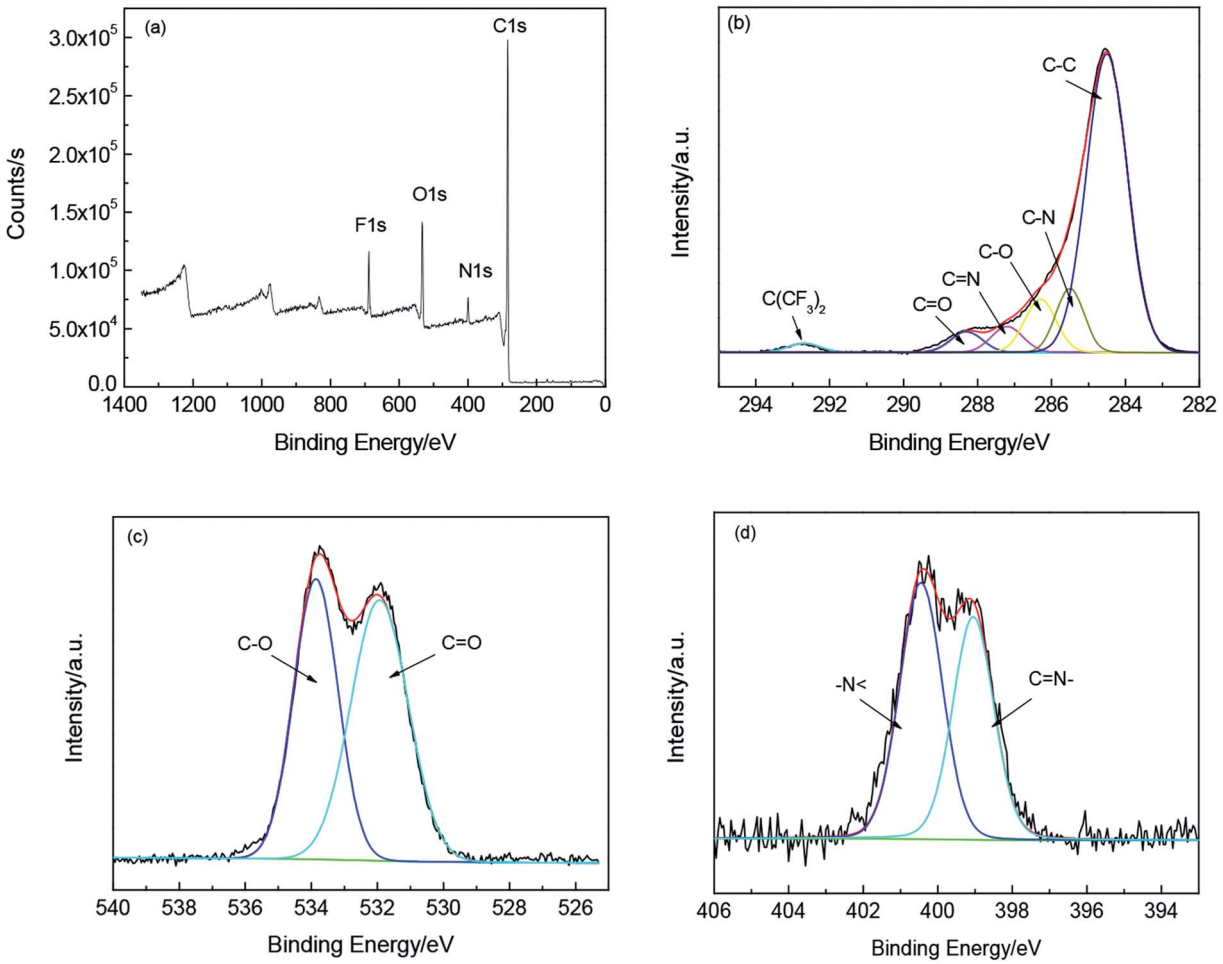

Fig. 8 XPS spectra of PEBO–6FDA (a)wide scan spectra; (b) fitting curves of C; (c) fitting curves of O; (d) fitting curves of N.

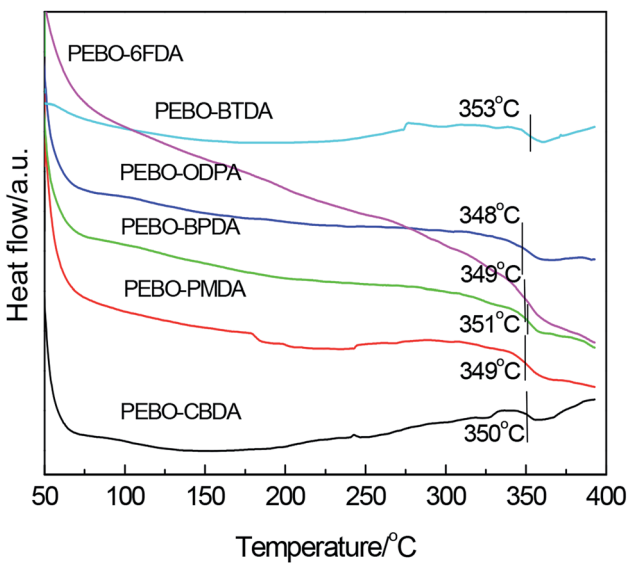

Fig. 9 DSC curves of PEBO membranes.

As previously described, gas transport properties of TR polymers strongly depended on the thermal treatment protocol. Four gas permeabilities of HPEI–6FDA increased with the increase of treatment temperature. When the treatment temperature was 450 °C, the H_2, CO_2, O_2 and N_2 permeabilities of PEBO–6FDA reached 239.6, 196.04, 46.41 and 9.25 Barrers, separately. Meanwhile the reasonable ideal selectivities CO_2/N_2 of 21.19 and O_2/N_2 of 5.02 make the TR a more attractive gas separation membrane. The significant increase in gas

Table 3 Gas separation performance of HPEI–6FDA treated at different temperatures

	Gas permeability[a]/Barrer[b]				Ideal selectivity[c]	
Samples	H_2	O_2	N_2	CO_2	CO_2/N_2	O_2/N_2
HPEI–6FDA	9.46	1.47	0.36	7.12	19.78	4.08
HPEI–6FDA-350	67.23	9.93	2.33	49.28	21.15	4.26
HPEI–6FDA-400	89.85	13.94	3.24	65.58	20.24	4.30
HPEI–6FDA-450	239.6	46.41	9.25	196.04	21.19	5.02

[a] All permeation results were obtained at 30 °C and 0.1 MPa. [b] 1 Barrer $= 10^{-10}$ cm^3 (STP) cm cm^{-2} s^{-1} cmHg $= 3.35 \times 10^{-16}$ mol m m^{-2} s^{-1} Pa. [c] Ideal selectivities were obtained by the ratio of two gas permeabilities.

Table 4 Gas separation properties of PEBO membranes (450 °C)

Samples	Permeability[a]/Barrer[b]				Ideal selectivity[c]		
	H_2	O_2	N_2	CO_2	CO_2/N_2	O_2/N_2	H_2/N_2
PEBO–CBDA	65.08	11.53	2.33	55.64	23.88	4.95	27.9
PEBO–PMDA	99.38	18.46	3.25	87.04	26.78	5.68	30.6
PEBO–BPDA	116.72	21.82	5.07	107.88	21.28	4.30	23.0
PEBO–ODPA	43.06	9.43	1.20	35.31	29.42	7.86	35.9
PEBO–BTDA	78.49	16.47	2.35	68.38	29.10	7.01	33.4
PEBO–6FDA	272.34	60.73	10.58	245.04	23.16	5.74	25.7
PEBO–6FDA-450 (ref. 36)	95.3	10.0	1.89	41.4	21.9	5.3	50.4
PBO–6FDA-450 (ref. 37)	371	54.2	11.8	255	21.6	4.6	31.4
PBO–TDA1-460 (ref. 28)	1547	311	58	1328	22.9	5.4	27
PBO-*co*-PI-6FDA-450 (ref. 49)	762	141	34	667	19.6	4.2	22

[a] All permeation results were obtained at 30 °C and 0.01 MPa. [b] 1 Barrer = 10^{-10} cm^3 (STP)cm cm^{-2} s^{-1} cmHg = 3.35×10^{-16} mol m m^{-2} s^{-1} Pa. [c] Ideal selectivities were obtained by the ratio of two gas permeabilities.

permeability was ascribed to a higher conversion rate of thermal rearrangement. Moreover, the permeabilities of four kinds of gases followed the order: H_2 (2.89 Å) > CO_2 (3.30 Å) > O_2 (3.46 Å) > N_2 (3.64 Å), which was in accordance to their kinetic diameters. Therefore, the thermal treatment protocol can significantly alter the gas separation performance of TR polymers.

According to the TG-MS results, the T_{TR}s of HPEI precursors were mainly around 400 °C, so the degree of thermal rearrangement should be relatively high when the heat treatment temperature was set at 450 °C. As expected according to the XRD curves, PEBO–6FDA exhibited the largest *d*-spacing value among these PEBOs, mainly due to the steric hindrance structure of hexafluoroisopropane. Therefore, it is distinct that the gas permeabilities order was as follows: PEBO–6FDA > PEBO–BPDA > PEBO–PMDA > PEBO–BTDA > PEBO–CBDA > PEBO–ODPA. Furthermore, it could be noticed that for every TR polymer in this study, four gas permerbilities follows the order: H_2 > CO_2 > O_2 > N_2. By comparing the gas selectivities, it was found that the CO_2/N_2 and O_2/N_2 ideal selectivities of PEBO–BTDA and PEBO–ODPA were higher than other PEBOs, but their gas permeabilities were very low probably because of intermolecular crosslinking. Integrally, PEBO–6FDA displayed O_2 permeability of 60.73 Barrer coupled with an O_2/N_2 selectivity of 5.74 and CO_2 permeability of 245.04 Barrer with a CO_2/N_2 selectivity of 23.16. The gas permeation properties of PEBO–6FDA are compared to data of previously reported PEBO[36] from 6FBAHPPF and 6FDA in Table 4. Clearly, the gas permeabilities and ideal selectivities of PEBO–6FDA from bis-AHPPF membrane were superior to 6FBAHPPF based PEBO. However, compared with some 6FDA-based and triptycene-based PBO without ether linkage,[28,37,49] the PEBO–6FDA showed lower gas permeabilities and higher CO_2/N_2 and O_2/N_2. The results implied that the bis-AHPPF based PEBO–6FDA exhibited moderate molecular chain rigidity, which was conducive to the balance of gas permeability and selectivity.

In addition, the data in Table 3 were measured at 0.10 MPa, while those in Table 4 were measured at 0.01 MPa. The gas separation tests were conducted with the unsupported membranes. Considering the poor mechanical properties of PEBO membranes after heat treatment, in order to obtain the gas permeability data of six kinds of TR polymers as many as possible, no higher pressure was set. For PEBO–6FDA (450 °C) under 0.01 MPa test pressure, the gas permeabilities of H_2, O_2, N_2 and CO_2 increased by 13.7%, 99.7%, 14.4% and 25.0% separately compared to 0.1 MPa. Namely, the gas permeability reduced as the feed pressure increased. Moreover, the selectivities of CO_2/N_2 and O_2/N_2 were also improved because the increases of O_2 and CO_2 were greater than that of N_2. This result is consistent with some literature reports.[50–52] This can be rationalized by a decrease in gas solubility coefficient with pressure as is typically observed in glassy polymers due to their dual-mode sorption behavior.

An ideal gas separation membrane is expected to have both high permeability and high selectivity. As illustrated in Fig. 10, the O_2/N_2 separation performance of PEBOs still showed a trade-off relationship between gas permeability and ideal selectivity. Compared to the literatures,[36,37,49] PEBO–ODPA,

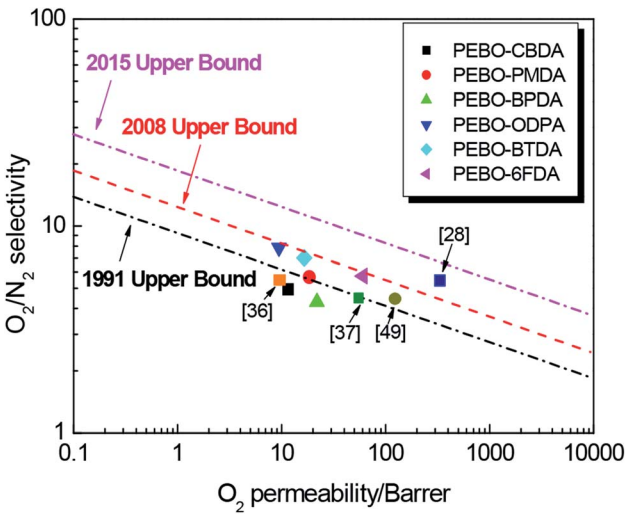

Fig. 10 Relationship between O_2 permeability and O_2/N_2 selectivity of PEBO membranes.

PEBO–BTDA and PEBO–6FDA were near or beyond the 2008 trade-off line. Especially, PEBO–6FDA exhibited much higher gas permeability for O_2/N_2 because of the bulky cardo and $-(CF_3)_2-$ moiety in the TR polymer backbone. Therefore, the diamine bis-AHPPF is effective for lowing thermal rearrangement temperature and adjusting the gas permeability and selectivity, and the corresponding PEBO membranes are expected to be applied in the field of gas separation.

4. Conclusions

In this work, a series of poly(ether-benzoxazole) (PEBO) membranes were prepared by thermal rearrangement of the hydroxy-containing poly(ether-imide)s (HPEI) from the diamine 9,9-bis[4-(4-amino-3-hydroxylphenoxy)phenyl]fluorene (bis-AHPPF) and six commerical dianhydrides CBDA, PMDA, BPDA, ODPA, BTDA as well as 6FDA, respectively *via* two-step thermal imidization method. It was found that the HPEI precursors exhibited excellent film formation, mechanical properties and thermal properties as well as lower T_{TR}. The thermal rearrangement (TR) reaction of all HPEIs were proved by FTIR, TGA-MS and XPS. Gas permeation data demonstrated that the gas permeabilities of TR membranes from HPEI–6FDA increased with the increase of thermal treatment temperature. Among six PEBOs, PEBO–6FDA displayed highest gas permeabilities with higher gas selectivities. When the testing pressure was 0.01 MPa, H_2, O_2, N_2 and CO_2 permeabilities of PEBO–6FDA were 272.34, 60.73, 10.58 and 245.04 Barrer respectively coupled with a selectivity CO_2/N_2 of 23.16 and a selectivity O_2/N_2 of 5.74, which were very near the 2008 upper bound of O_2/N_2. The diamine bis-AHPPF can effectively decrease the thermal rearranged temperature and improve the mechanical properties and processability. Therefore, the PEBO–6FDA membranes exhibit moderate gas permeabilities and selectivities, which are expected to be applied as high performance membrane materials in gas separation field.

Conflicts of interest

There are no conflicts of interest to declare.

Acknowledgements

This work was financially supported by the National Natural Science Foundation of China (Grant number: 21878033, 21406102), Natural Science Foundation of Liaoning Province (Grant number: 20180550439) and University of Science and Technology Liaoning Talent Project Grants (Grant number: 601011507-17).

References

1 M. Galizia, W. S. Chi, Z. P. Smith, T. C. Merkel, R. W. Baker and B. D. Freeman, *Macromolecules*, 2017, **50**, 7809–7843.
2 H. A. Abdulgader, V. Kochkodan and N. Hilal, *Sep. Purif. Technol.*, 2013, **116**, 253–264.
3 Y. Hu, X. Li, L. Yan and B. Yue, *Fuel Cells*, 2017, **17**, 3–17.
4 X. Zou and G. Zhu, *Adv. Mater.*, 2017, **30**, 1700750–1700763.
5 H. Shamsipur, B. A. Dawood, P. M. Budd, P. Bernardo, G. Clarizia and J. C. Jansen, *Macromolecules*, 2014, **47**, 5595–5606.
6 P. Gabrielli, M. Gazzani and M. Mazzotti, *J. Membr. Sci.*, 2017, **526**, 118–130.
7 D. J. Liaw, K. L. Wang, Y. C. Huang, K. R. Lee, J. Y. Lai and C. S. Ha, *Prog. Polym. Sci.*, 2012, **37**, 907–974.
8 Y. Jung, B. Jeong, Y. Yang, T. Kim and S. Kwon, *Macromol. Res.*, 2017, **25**, 971–975.
9 S. W. Yeom, B. You, K. Cho, H. Y. Jung, J. Park, C. Shin, B. K. Ju and J. W. Kim, *Sci. Rep.*, 2017, **7**, 3438–3447.
10 Z. Wang, A. P. Isfahani, K. Wakimoto, B. B. Shrestha, A. Muchtar, D. Yamaguchi, B. Ghalei and E. Sivaniah, *ChemSusChem*, 2018, **11**, 2744–2751.
11 S. Kim, X. Wang, S. Ando and X. Wang, *RSC Adv.*, 2014, **4**, 27267–27276.
12 Y. Wu, C. Shi, Z. Chen, Y. Zhou, S. Liu and J. Zhao, *Polym. Chem.*, 2019, **10**, 1399–1406.
13 W. W. Lee, J. Y. Hwang, M. K. Choi, D. H. Suh and D. S. Seo, *Ferroelectrics*, 2006, **344**, 51–61.
14 X. Ma, R. Swaidan, Y. Belmabkhout, Y. Zhu, E. Litwiller, M. Jouiad, I. Pinnau and Y. Han, *Macromolecules*, 2012, **45**, 3841–3849.
15 H. B. Park, C. H. Jung, Y. M. Lee, A. J. Hill, S. J. Pas, S. T. Mudie, E. Van Wagner, B. D. Freeman and D. J. Cookson, *Science*, 2007, **318**, 254–258.
16 C. A. Scholes, *Aust. J. Chem.*, 2016, **69**, 601–611.
17 T. Woock, S. Bjorgaard, B. Tande and A. Alshami, *Membr. Technol.*, 2016, **10**, 7–12.
18 D. Meis, A. Tena, S. Neumann, P. Georgopanos, T. Emmler, S. Shishatskiy, S. Rangou, V. Filiz and V. Abetz, *Polym. Chem.*, 2018, **9**, 3987–3999.
19 D. F. Sanders, R. Guo, Z. P. Smith, Q. Liu, K. A. Stevens, J. E. McGrath, D. R. Paul and B. D. Freeman, *Polymer*, 2014, **55**, 1636–1647.
20 C. H. Park, E. Tocci, Y. M. Lee and E. Drioli, *J. Phys. Chem. B*, 2012, **116**, 12864–12877.
21 G. Dong and Y. M. Lee, *Comprehensive Membrane Science and Engineering*, Elsevier Science, 2017, pp. 190–215.
22 S. H. Han, N. Misdan, S. Kim, C. M. Doherty, A. J. Hill and Y. M. Lee, *Macromolecules*, 2010, **43**, 7657–7667.
23 M. Calle, A. E. Lozano and Y. M. Lee, *Eur. Polym. J.*, 2012, **48**, 1313–1322.
24 D. F. Sanders, R. Guo, Z. P. Smith, K. A. Stevens, Q. Liu, J. E. McGrath, D. R. Paul and B. D. Freeman, *J. Membr. Sci.*, 2014, **463**, 73–81.
25 R. J. Swaidan, X. Ma and I. Pinnau, *J. Membr. Sci.*, 2016, **520**, 983–989.
26 N. Alaslai, X. Ma, B. Ghanem, Y. Wang, F. Alghunaimi and I. Pinnau, *Macromol. Rapid Comm.*, 2017, **38**, 1700303–1700308.
27 C. Aguilar-Lugo, C. lvarez, Y. M. Lee, J. Campa and A. E. Lozano, *Macromolecules*, 2018, **51**, 1605–1619.
28 F. Alghunaimi, B. Ghanem, Y. Wang, O. Salinas, N. Alaslai and I. Pinnau, *Polymer*, 2017, **121**, 9–16.

29 B. Comesana-Gandara, J. G. Campa, A. Hernandez, H. J. Jo, Y. M. Lee, J. Abajo and A. E. Lozano, *RSC Adv.*, 2015, **5**, 102261–102276.
30 A. Tena, S. Rangou, S. Shishatskiy, V. Filiz and V. Abetz, *Sci. Adv.*, 2016, **2**, 1501859–1501868.
31 R. Guo, D. F. Sanders, Z. P. Smith, B. D. Freeman, D. R. Paul and J. E. McGrath, *J. Mater. Chem. A*, 2013, **1**, 6063–6072.
32 A. Kushwaha, M. E. Dose, Z. P. Smith, S. Luo, B. D. Freeman and R. Guo, *Polymer*, 2015, **78**, 81–93.
33 S. Luo, J. Liu, H. Lin, B. A. Kazanowska, M. D. Hunckler, R. K. Roeder and R. Guo, *J. Mater. Chem. A*, 2016, **4**, 17050–17062.
34 C. A. Scholes, C. P. Ribeiro, S. E. Kentish and B. D. Freeman, *J. Membr. Sci.*, 2014, **450**, 72–80.
35 L. M. Robeson, M. E. Dose, B. D. Freeman and D. R. Paul, *J. Membr. Sci.*, 2017, **525**, 18–24.
36 M. Calle and Y. M. Lee, *Macromolecules*, 2011, **44**, 1156–1165.
37 Y. F. Yeong, H. Wang, K. P. Pramoda and T. S. Chung, *J. Membr. Sci.*, 2012, **397–398**, 51–65.
38 Y. Lu, J. Hao, L. Li, J. Song, M. Fei, G. Xiao, H. Zhao, Z. Hu and T. Wang, *Acta Polym. Sin.*, 2016, **8**, 1145–1150.
39 Y. Lu, J. Hao, L. Li, J. Song, G. Xiao, H. Zhao, Z. Hu and T. Wang, *React. Funct. Polym.*, 2017, **119**, 134–144.
40 B. M. Lee, D. J. Kim and S. Y. Nam, *J. Nanosci. Nanotech.*, 2015, **15**, 2351–2355.
41 Y. Kobayashi, S. Kazama, K. Inoue, T. Toyama, Y. Nagai, K. Haraya, H. F. M. Mohamed, B. E. O'Rouke, N. Oshima, A. Kinomura and R. Suzuki, *J. Phys. Chem. B*, 2014, **118**, 6007–6014.
42 A. A. Alghannam, G. O. Yahaya, A. Hayek, I. Mokhtari, Q. Saleem, D. A. Sewdan and A. A. Bahamdan, *J. Membr. Sci.*, 2018, **553**, 32–42.
43 C. Zhang, B. Cao and P. Li, *J. Membr. Sci.*, 2018, **546**, 90–99.
44 S. Kim and Y. M. Lee, *Prog. Polym. Sci.*, 2015, **43**, 1–32.
45 Y. Lu, J. Hao, G. Xiao, L. Li, Z. Hu and T. Wang, *High Perform. Polym.*, 2019, **31**, 1101–1111.
46 J. Y. Park and D. R. Paul, *J. Membr. Sci.*, 1997, **125**, 23–39.
47 M. Calle, Y. Chan, H. J. Jo and Y. M. Lee, *Polymer*, 2012, **53**, 2783–2791.
48 Q. Liu, D. R. Paul and B. D. Freeman, *Polymer*, 2016, **82**, 378–391.
49 S. Luo, Q. Zhang, T. K. Bear, T. E. Curtis, R. K. Roeder, C. M. Doherty, A. J. Hill and R. Guo, *J. Membr. Sci.*, 2018, **551**, 305–314.
50 Y. Zheng, Y. Wu, B. Zhang and Z. Wang, *J. Appl. Polym. Sci.*, 2020, **137**, 48398.
51 B. Zhang, C. Yang, S. Liu, Y. Wu, T. Wang and J. Qiu, *Micropor. Mesopor. Mat.*, 2019, **285**, 142–149.
52 R. Xu, L. Li, X. Jin, M. Hou, L. He, Y. Lu, C. Song and T. Wang, *J. Membr. Sci.*, 2019, **586**, 306–317.